European Journal of Pharmaceutics and Biopharmaceutics 136 (2019) 1–8

Contents lists available at ScienceDirect

European Journal of Pharmaceutics and Biopharmaceutics

journal homepage: www.elsevier.com/locate/ejpb

Research paper

Polymeric nanoparticles for the delivery of miRNA to treat Chronic Obstructive Pulmonary Disease (COPD)

Adel Mohamed[a], Nitesh K. Kunda[b], Kehinde Ross[a], Gillian A. Hutcheon[a], Imran Y. Saleem[a,*]

[a] Liverpool John Moores University, School of Pharmacy and Biomolecular Sciences, Liverpool L3 3AF, UK
[b] Department of Pharmaceutical Sciences, College of Pharmacy and Health Sciences, St. John's University, Jamaica, NY, USA

ARTICLE INFO

Keywords:
Nanoparticles
microRNA (miRNA)
miR-146a
Chronic Obstructive Pulmonary Disease (COPD)
Interleukin-1 receptor-associated kinase 1 (IRAK1)
RNA interference (RNAi)
Inflammation

ABSTRACT

RNA interference (RNAi) based therapeutics are considered an endogenous mechanism for modulating gene expression. In addition, microRNAs (miRNAs) may be tractable targets for the treatment of Chronic Obstructive Pulmonary Disease (COPD). In this study miR146a was adsorbed onto poly (glycerol adipate-co-ω-pentadecalactone), PGA-co-PDL, nanoparticles (NPs) to reduce target gene IRAK1 expression. NPs were prepared using an oil-in-water single emulsion solvent evaporation method incorporating cationic lipid dioleoyltrimethylammoniumpropane (DOTAP). This resulted in NPs of 244.80 ± 4.40 nm at 15% DOTAP concentration, zeta potential (ZP) of +14.8 ± 0.26 mV and miR-146a (40 μg/ml) maximum adsorption onto 15% DOTAP NPs was 36.25 ± 0.35 μg per 10 mg NP following 24 h incubation. Using the MTT assay, it was observed that over 75% at 0.312 mg/ml of A549 cells remained viable after 18 h exposure to cationic NPs at a concentration of 1.25 mg/ml. Furthermore, the *in vitro* release profile of miR-146a from loaded NPs showed a continuous release up to 77% after 24 h. Internalization of miR-146a loaded cationic NPs was observed in A549 cell lines using fluorescence and confocal microscopy. The miR146a delivered as miR-146a-NPs had a dose dependent effect of highest NPs concentrations 0.321 and 0.625 mg/ml and reduced target gene IRAK1 expression to 40%. In addition, IL-8 promoter reporter output (GFP) was dampened by miR-146a-NPs. In conclusion, miR-146a was successfully adsorbed onto PGA-co-PDL-DOTAP NPs and the miR-146a retained biological activity. Therefore, these results demonstrate the potential of PGA-co-PDL NPs as a delivery system for miR-146a to treat COPD.

1. Introduction

Chronic obstructive pulmonary disease (COPD) is a major cause of morbidity and mortality and is currently the fourth leading cause of death in the world and predicted to become the third leading cause of chronic illness and death by 2030 [1]. The World Health Organization (WHO) estimated that more than 3 million people died of COPD in 2012, which is equivalent to 6% of all deaths globally that year [1]. Moreover, the Global Initiative on Obstructive Lung Disease (GOLD) indicated the disease is more prevalent among males than females [2]. Current therapeutic strategies to reduce COPD (bronchodilators, antibiotics, inhaled corticosteroids and oxygen) [3] have not been shown to delay or correct the long term advancement of COPD [2].

Mature microRNAs (miRNAs) are small noncoding RNA molecules (≈22 nucleotides long) that downregulate gene expression, first through acute translational repression but subsequently by steady-state mRNA destabilisation [4]. Therapeutic interventions based on modulation of miRNA levels have emerged as a tractable approach for clinical intervention in respiratory diseases [5–7]. In particular, miR-146a has been linked to COPD pathogenesis [8,9]. The ability of miR-146a to downregulate the interleukin 1 receptor (IL-1R) and Toll-like receptor (TLR) signalling components IL-1 receptor-associated kinase (IRAK1) and tumour necrosis factor (TNF) receptor-associated factor (TRAF6) supports negative feedback regulation of IL-1β, IL-6 and IL-8 [10,11]. However, one of the main concerns regarding targeting inflammatory lung disease is that upon delivery of the naked, negatively charged miRNAs to the site of action, the molecules cannot cross the anionic cell membranes [12].

Nanoparticles (NPs) have potential to overcome this problem and altering the surface charge to be cationic can enhance the interaction with negative miRNA and particle uptake into cells [13]. NPs prepared from traditional biodegradable polymers such as poly (lactic-co-glycolic acid) (PLGA) or poly (glycerol adipate-co-ω-pentadecalactone) (PGA-co-PDL) can be used for gene delivery and specific cell targeting by coating the NPs with cationic materials [14] or incorporating cationic surfactants [13]. Nucleic acids can bind and adsorb onto the cationic

* Corresponding author at: Liverpool John Moores University, School of Pharmacy & Biomolecullar Sciences, Byrom Street, Liverpool L3 3AF, UK.
E-mail address: i.saleem@ljmu.ac.uk (I.Y. Saleem).

https://doi.org/10.1016/j.ejpb.2019.01.002
Received 30 July 2018; Received in revised form 4 December 2018; Accepted 3 January 2019
Available online 04 January 2019
0939-6411/

NPs via electrostatic interactions. The difficulty in loading of miRNA into NPs can be attributed to the hydrophobic nature of NPs and the absence of electrostatic interaction between miRNA and NPs. Studies revealed that additionally attaching molecules such as chitosan or cationic lipids such as dioleoyltrimethylammonium propane (DOTAP) promote siRNA transfection efficacy [15]. These cationic additives can be added to the NPs' surface pre or post formation [16].

PGA-co-PDL NPs have previously been investigated for the delivery of proteins and vaccines either by encapsulation of the molecules within the particle or adsorption to the surface [17–20]. In this study, we optimised the formulation of the NPs with surface adsorbed miR-146a for delivery to lung epithelial cells and then evaluated the toxicity, *in vitro* release, cell uptake, and biological activity.

2. Materials and methods

2.1. Materials

Poly (vinyl alcohol) PVA, Mw of 13–23 kDa 87–89% hydrolysed was purchased from Clariant GmbH, Frankfurt am Main, Germany), Novozyme 435 (a lipase from *Candida antartica* immobilized on a microporous acrylic resin) from Biocatalytics, USA and DOTAP from Avanti Polar lipids, Alabaster, AL, USA. Solvents were purchased from Fischer chemicals (Fischer Scientific, UK). RPMI-1640 medium with L-glutamine and $NaHCO_3$, thiazoly blue tetrazolium bromide (MTT), Nile red and RNase-free diethyl pyrocarbonate (DEPC) water were purchased from Sigma Aldrich, UK. A synthetic miR-146a mimic with a FAM-label on the sense 5′ FAM-CCGGGCAAUUCAGUUUCUACA-dTdT-3′, was purchased from Eurogenetec, UK with the sequence: sense 5′ FAM-CCGGGCAAUUCAGUUUCUACA-dTdT-3′, antisense 5′ dTdT-GGC CCGUUAAGUCAAAGAUGU-3′.

2.2. Methods

2.2.1. Nanoparticle preparation and miRNA adsorption

PGA-co-PDL NPs were prepared using an oil-in-water (o/w) single emulsion method, incorporating 0.4 mg Nile Red dye in the inner organic phase (dichloromethane, DCM) for visualization experiments aqueous phase contained 10% w/v poly (vinyl alcohol), (PVA) as previously described [13]. Indicated concentrations of DOTAP (5, 10, 15, 20, and 25% w/w of the polymer) were added to the organic phase to prepare cationic NPs. The FAM-labelled miR-146a mimic (40, 30, 20 and 10 μg, respectively) was added to 1 ml solution of RNase free water containing 10 mg of NPs (to obtain a final NP:miRNA weight ratio of 250:1) and mixed using a HulaMixer Sample Mixer (Life Technologies, UK) at 20 rpm and 25 °C at staggered time points (0.5, 1, 2, 4 and 24 h). After adsorption, RNase free water was added to a total volume of 4 ml prior to separation of free miR-146a from the adsorbed miR-146a by ultracentrifugation at 35,000*g*, for 40 min at 4 °C using an Optima L-80 Ultracentrifuge (Beckman, UK).

2.2.2. Particle size and zeta potential

The mean particle size and polydispersity index (PDI) of the NPs were analysed by dynamic laser scattering, and the surface charge of the particles determined by analysis of the zeta-potential using a Zetasizer Nano ZS, Malvern Instruments Ltd, UK. The NPs (10 mg) were diluted with 4 ml distilled water and 1 ml of the diluted sample was loaded into a measuring cuvette.

2.2.3. miRNA adsorption characterisation

The concentration of adsorbed miR-146a was determined indirectly from the difference in miR-146a concentration before and after loading by UV absorbance at 260 nm using a NanoDrop 2000C (Thermo Fisher Scientific, and USA). Furthermore, the concentration of FAM labelled miR-146a was determined by fluorescence using a plate reader (CLARIOstar®) at λ_{ex}: 495 nm; λ_{em}; 520 nm. In both cases, a calibration curve was generated using known concentrations of miR-146a.

2.2.4. In vitro release

The miR-146a-adsorbed PGA-co-PDL NPs (10 mg) were suspended in 4 ml PBS (pH 7.4) and incubated at 37 °C with rotation at 20 rpm on a HulaMixer, samples were centrifuged (Beckman L-80 Ultracentrifuge, UK) at 35,000*g* for 40 min and 1 ml of supernatant was collected for quantification. The particles were re-suspended in 1 ml PBS and incubation resumed. The absorbance of the supernatant was measured on a Nanodrop spectrophotometer at 260 nm. The amount of released miR-146a was calculated as a percentage of cumulative released miR-146a to the total amount of adsorbed miR-146a.

$$\%\ \text{Cumulative miR-146a released} = \frac{\text{Cumulative miR-146a released}}{\text{miR-146a loaded}} \times 100$$

The % cumulative miR-146a release was assessed using zero order, first order and Higuchi's square root plot release models. The correlation coefficient was calculated from the following graphical representations, zero order: *% cumulative miR-146a release versus time*; first order: log *% cumulative miR-146a remaining versus time*; Higuchi: *% cumulative miR-146a release versus square root of time.*

2.2.5. Cell culture and toxicity studies

Human alveolar adenocarcinoma A549 cells (ATCC, LGC Standards, Europe) were maintained at 37 °C and 5% CO_2 in RPMI-1640 medium with 100 U/ml penicillin, 100 μg/ml streptomycin, 2 mM L-glutamine and 10% fetal bovine serum (FBS). Cytotoxicity was determined *in vitro* using the MTT assay. Cells were seeded in 96 well plates in growth medium at a density of 1.2×10^5 cells per well. After 18 h (80% confluence), the cells were incubated for a further 24 h with 100 μl of premixed freshly prepared cationic NPs and non-cationic NPs (control) at range of concentrations (0–2.5 mg/ml), and 10% dimethyl sulfoxide (DMSO) as a positive control. The medium was removed after 18 h and 40 μl of the MTT solution (5 mg/ml in PBS) added to each well for 2 h at 37 °C, followed by removal of MTT medium and the formazan dissolved in 100 μl DMSO. The absorbance was measured at 570 nm and the cell viability percentage calculated as the absorbance ratio between NPs treated and non-treated cells (control).

2.2.6. Cell imaging

Cells (5×10^5 cells per well) were seeded in an 8 well chambered slide (Fisher Scientific, UK) and incubated overnight (37 °C, 5% CO_2). Culture media was replaced with 500 μl of FAM-labelled miR-146a-NPs and Nile Red labelled NPs in serum free medium for 1 h. Cells were then washed with PBS and fixed using 4% paraformaldehyde (PFA), or ice-cold (−20 °C) 100% methanol was used for 15 min. Permeabilization of the PFA-treated samples was performed with 0.1% Triton-X 100 for 10–15 min at room temperature. Nuclear counter-staining was performed with 1 μg/ml DAPI for 5 min. Confocal images were acquired using a Zeiss LSM 710 confocal laser scanning microscope equipped with an argon ion laser. Using the 488 nm laser line for FAM labelled miR-146a and 543 nm line Nile Red labelled NPs.

2.2.7. Semi-quantitative reverse transcriptase PCR

Cells (3.8×10^5 cells per well) were incubated in serum free medium with miR-146a-NPs for 1 h. The miR-146a-NPs mixture was replaced with complete medium and the cells incubated for 24 h. Total RNA was extracted using the RNeasy Mini kit according to the manufacturer's instructions. Reverse transcription for cDNA generation was performed on 200 ng RNA using miScript reagents (Qiagen, Manchester, UK). Levels of *IRAK1* transcripts, were assessed using RT^2 qPCR Primer Assays in 20 μl reactions composed of 10 μl SYBR Green PCR master mix, 2 μl primers, 2 μl diluted cDNA and water to 20 μl. The reactions were amplified for three-step method. Expression was normalised to glyceraldehyde-3-phosphate dehydrogenase (*GAPDH*) using

the $2^{-\Delta\Delta Ct}$ method [21], SYBR Green PCR reagents and PCR primers were purchased from Qiagen (Manchester, UK).

2.2.8. Immunoblotting: Western blots

Cells (3.8×10^5 cells per well) were seeded on a 6 well plate. After 24 h growth, the cells were incubated in serum free medium with 1 ml of pre-mixed freshly prepared miR146a-NPs at range of concentrations (0–0.625 mg/ml) for 1 h. The miR-146a-NPs was then replaced with complete medium and the cells incubated for 24 h and 48 h respectively. The cells were rinsed with PBS, and lysed on ice by replacing the culture medium in RIPA buffer containing 150 mM sodium chloride, 1% Triton X-100, 0.5% sodium deoxycholate, 0.1% sodium dodecyl sulphate (SDS), 50 mM Tris pH 8.0, sodium orthovandate and protease inhibitor tablet (Roche). The protein extract was determined using BCA assay (Sigma, UK). Samples (4 parts) were diluted with an equal volume of 1 part Laemmli buffer (0.5 M Tris-HCL pH 6.8, glycerol, SDS, 0.25% bromophenol blue, B-mercaptoethanol) and boiled for 5 min at 95 °C. Protein lysate (20 μg for each lane) were resolved on 12% precast gel (Bio-Rad, UK) and transferred to nitrocellulose membranes in Tris-glycine buffer with 20% methanol. Following transfer, membranes were blocked for 1 h at RT in 5% fat free milk in TBST (TBS and Tween-20) before probing overnight at 4 °C with antibodies anti-IRAK1 (1:1000, Abcam), β-Actin (1:1000, ThermoFischer). Membranes were washed three times in TBST then incubated with horseradish Peroxidase conjugated secondary antibodies (1:5000, sigma) for 1 h at room temperature. Membranes were subsequently washed three times and exposed in a chemiluminescence Pierce ECL reagents (Thermo Fisher, UK) according to manufacturer's protocol. Densitometry was performed using ImgaeJ software, and protein of interest values were used to normalize against β-Actin values.

2.2.9. IL-8 promoter reporter assay

Cells (5×10^5 cells per well) were seeded on an 8 well chambered slide (Fisher Scientific, UK) and incubated for 24 h prior to transfection. Transfections were performed using Lipofectamine 3000 reagent following the manufacturer's protocol (Life technology, UK) in serum free DMEM and a total amount of 0.5 μg of DNA per well was used. The DNAs used were pIL8/d2EGFP and pDsRED mono promoters, kind gifts from Professor Endre Kiss-Toth (University of Sheffield, UK). The cells were transfected for 6 h and then washed twice with PBS. A prepared mixture of unlabelled miR146a-NPs (100 μl) was added and incubated for 1 h. After this cells were washed twice in PBS then, cells were stimulated with 1 ng/ml IL-1β or TNFα and incubated for further 6 h. Cells were washed with PBS and subsequently fixed in −20 °C methanol and images acquired on an Olympus BX51 Fluorescent microscope.

2.2.10. Statistical analysis

The experiments were performed in triplicate and data is presented as mean ± standard deviation (SD) unless stated. Statistical differences were performed by One-way analysis of variance (ANOVA) using Minitab® with the Tukey's comparison at value $p < 0.05$.

3. Results

3.1. Formulation and characterisation

3.1.1. Particle size and zeta potential

NPs (± DOTAP) were prepared using a single emulsion solvent evaporation method by adding the DOTAP, if relevant, in the organic phase at different DOTAP and PGA-co-PDL weight ratios. The data presented in this study indicate that PGA-co-PDL mixed with DOTAP formed cationic NPs using 10–25% (w/w) DOTAP. It was noted that increasing the concentration of DOTAP decreased particle size and caused the zeta potential to become more positive (Fig. 1A). Varying the concentration of DOTAP incorporated into the PGA-co-PDL NPs resulted in a change in particle size from 266.10 ± 20.80 nm at 0% (w/w) DOTAP to 197.90 ± 1.70 nm at 20% (w/w) DOTAP and, a change in surface charge from −18.9 ± 0.9 mV to + 16.7 ± 0.1 mV that varied according to DOTAP concentration (Fig. 1B). However, there was little change in particle properties from 15% to 20% (w/w), so given the increased cost and toxicity of using higher DOTAP concentrations, 15% (w/w) DOTAP was chosen for all future work and was selected for the subsequent miR-146a adsorption studies.

miR-146a loaded cationic NPs (miR-146a-NP), showed no change in particle size compared to unloaded NPs (244.8 ± 4.4 nm and 242.4 ± 0.3 nm respectively). The charge after adsorption of miR-146a ranged between (+5.9 mV to +11.1 mV) for miR-146a NPs compared to +14.8 mV for unloaded NPs, showing the miR-146a loaded NPs were still positively charged. Furthermore, the reduction in zeta potential confirmed the miR-146a was adsorbed.

3.1.2. miR-146a adsorption

The 15% (w/w) DOTAP NPs were used to study miR-146a adsorption by first using a fixed miR-146a concentration (40 μg/ml) at different time points 0.5, 1, 2, 4 and 24 h (Fig. 1C). After 0.5 h, 12.05 ± 1.3 μg of miR-146a (40 μg/ml) was adsorbed on 10 mg NPs. The maximum miR-146a adsorption was 36.25 ± 0.35 μg miR-146a per 10 mg NPs after 24 h. Beyond 2 h there was no significant difference in miR-146a adsorption with a maximum of 32.25 ± 2.0 μg miR-146a per 10 mg NPs ($p < 0.05$, ANOVA/ Tukey's comparison).

Furthermore, adsorption of miR-146a at different concentrations with a fixed time of 2 h was investigated. As shown in (Fig. 1D) over 75% of miR-146a was adsorbed at concentrations of 20, 30 and 40 μg miR-146a. The positively charged NPs attract the negatively charged miR-146a by electrostatic interaction. Therefore, the results indicate that 15% (w/w) DOTAP NPs can be effectively adsorbed with miR-146a. Confirmation that the miR-146a was associated with the NPs was achieved using fluorescence microscopy, which indicated the fluorescently labelled NPs (Nile Red dye) with labelled FAM-miR-146a (green) (Fig. 2).

3.2. In vitro release and cytotoxicity

The *In vitro* release profile of the miR-146a -loaded NPs (40 μg/ml) showed that the miR-146a release could be divided into stages (Fig. 3). The miR-146a was initially rapidly released in the first 4 h with 51 ± 1.5% cumulative release. Followed by a second stage during which the miR-146a was continually released between 4 h up to 24 h, providing a cumulative release of 77 ± 1.5%. The correlation coefficient (r^2) of miR-146a release from NPs was 0.743 (zero order), 0.441 (first order) and 0.932 (Higuchi). The Higuchi diffusion model had the best correlation, hence, the release of the miR-146a from NPs seems to be a diffusion-limited process.

To assess the toxicity profile of the PGA-co-PDL NPs with DOTAP coated NPs, 15% (w/w) DOTAP particles investigated for toxicity equivalent in size to non-loaded NPs. Blank cells (control) had 100% cell viability, whereas cell viability at 1.25 mg/ml were around 90% (unloaded NPs) that decreased to 65% (15% DOTAP NPs) (Fig. 4), indicating the NPs appear to cause cell death with an increase in concentration after 18 h exposure [22,23].

3.3. Cellular uptake

To visualise the cellular uptake of the NPs for delivery to A549 cells, NPs encapsulating Nile red dye were prepared and added to A549 cells. The NPs were observed around the nucleus and in the cytoplasm, in large populations of cells and single cells, indicating that the NPs were taken up by the cells (Fig. 5A–C: fluorescence and D–F: confocal).

Furthermore, to visualize the intracellular uptake of FAM-labelled miR-146a-NPs for delivery to A549 cells, FAM-labelled miR-146a-NPs were prepared and exposed to A549 cells. Cells were stained with DAPI,

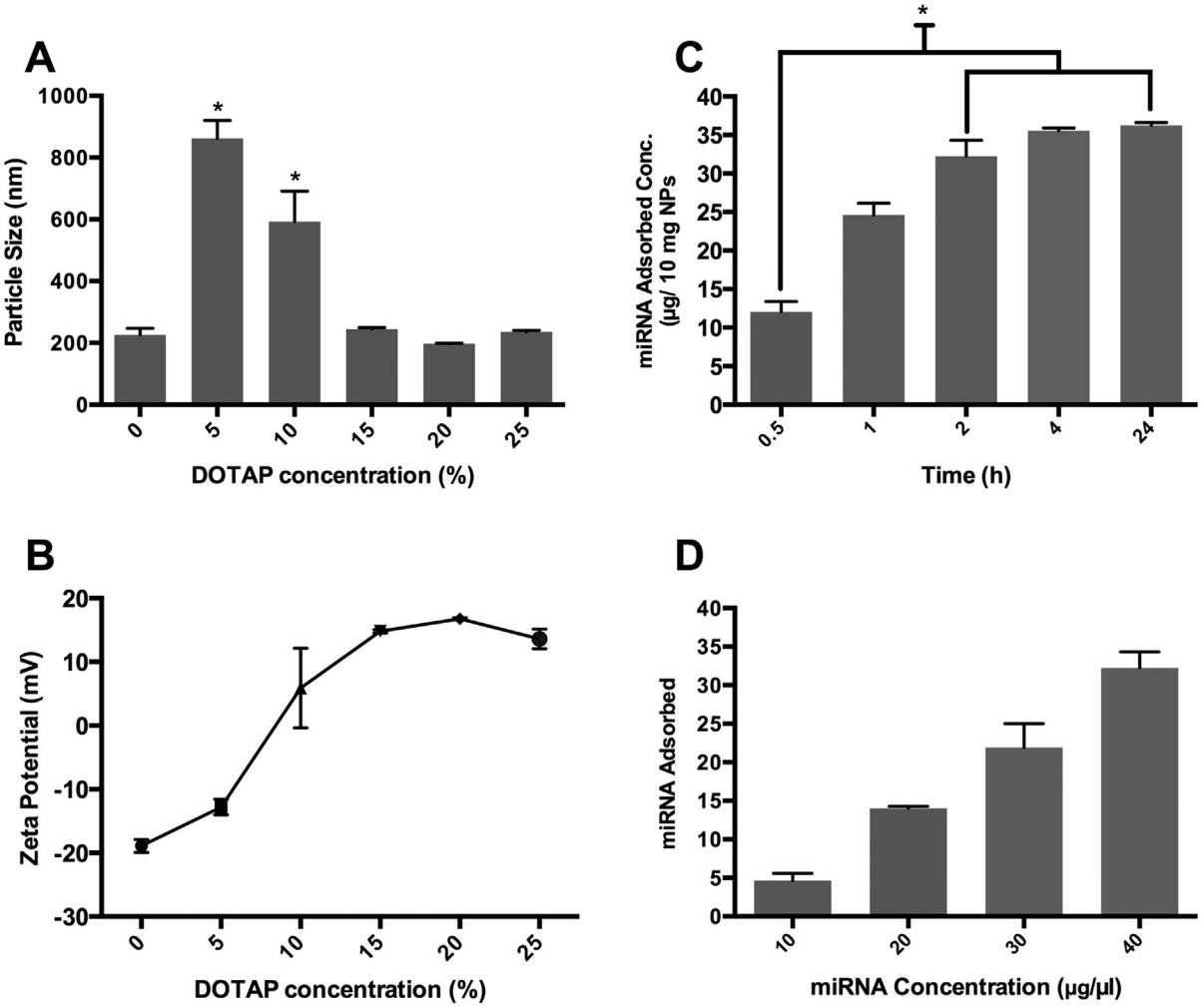

Fig. 1. (A) The effect of the concentration of DOTAP on particle size of PGA-co-PDL NPs, (B) The effect of the concentration of DOTAP on the particle surface charge of PGA-co-PDL NPs, (C) adsorption of miRNA (40 µg/ml) at different time points up to 24 h onto 15% DOTAP NPs, (D) miRNA adsorption onto 15% DOTAP NPs at various miRNA concentrations over 2 h, µg miRNA per 10 mg NPs. Data is represented in (A) and (B) as Mean ± SD (n = 3), (C) and (D) as Mean ± SD (n = 2). *p < 0.05, ANOVA/Tukey's comparison.

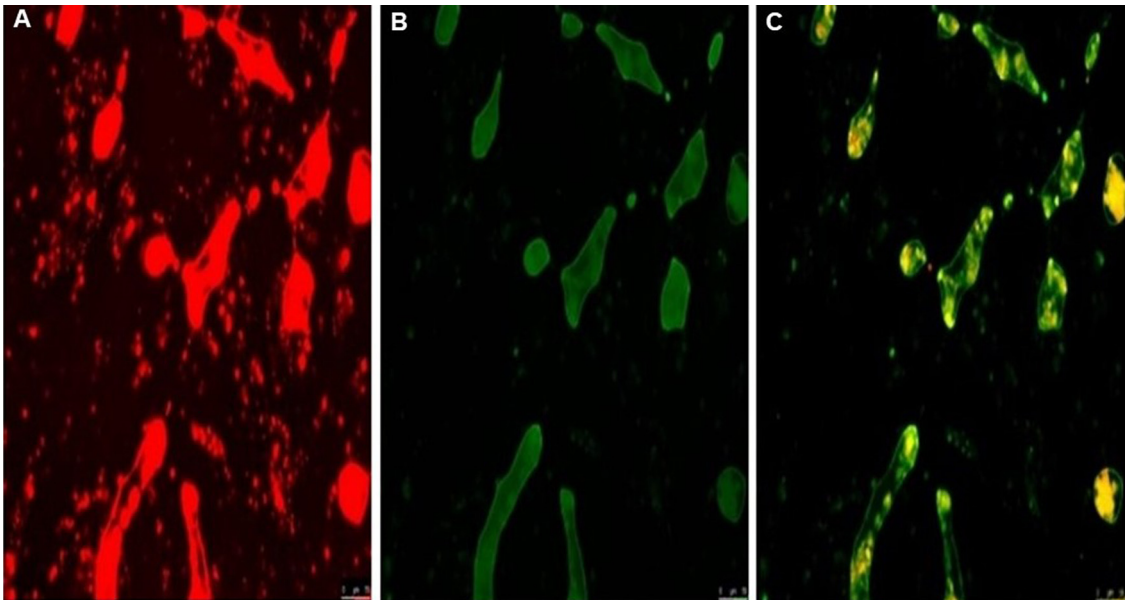

Fig. 2. Image (A) shows red colour NPs (Nile Red dye), (B) the labelled FAM-miRNA (Green) and (C) the merged image of both A and B (scale bar represent 50 µm). (For interpretation of the references to colour in this figure legend, the reader is referred to the web version of this article.)

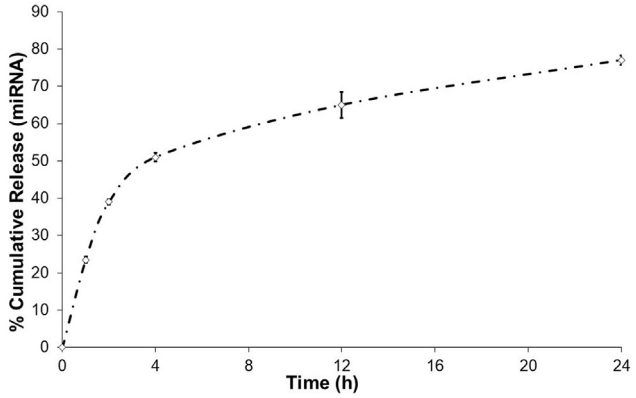

Fig. 3. miRNA *in vitro* release from 15% DOTAP NPs in phosphate buffer saline at pH 7.4. Data presented as Mean ± SD (n = 3).

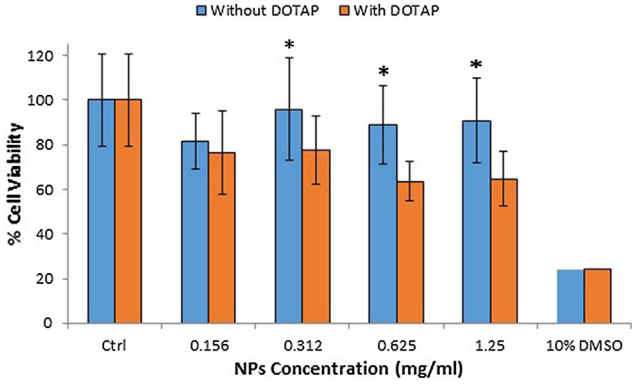

Fig. 4. Cytotoxic effect of unloaded NPs (0% DOTAP) and 15% DOTAP NPs on A549 cells after 18 h incubation. DMSO was used as positive control; the cell viability was measured using MTT assay. The experiments were repeated three times and data represented as mean ± SD (n = 3), *p < 0.05, ANOVA/Tukey's to compare NPs with and without DOTAP at concentrations (0.312 mg, 0.625 mg, and 1.25 mg/ml).

and particles were distributed differentially across a population of cells with a clear variation (Fig. 6A–C: fluorescence). The same results were obtained with a single cell where the particles can be observed around the nuclei and cytoplasm (Fig. 6D–F: confocal).

3.4. Effect of miR-146a-loaded NPs on target gene, protein expression and reporter assay

To confirm miR-146a-NP function, the expression of the target genes *IRAK1* was assessed in A549 cells. Analysis of transcript levels showed that miR-146a delivered via NPs (miR-146a mimic) and the highest NPs concentrations led to suppression of IRAK1 to 40%, compared with untreated cells (Fig. 7A). The expression of *IRAK1* was normalised to *GAPDH* expression.

To confirm the downregulation of *IRAK1* occurred at the protein levels, miR-146a-loaded NPs were applied to A549 cells and lysates evaluated by immunoblotting (Fig. 7B). The miR-146a-NPs reduced *IRAK1* protein levels in A549 cells after 24 h and 48 h treatment. The decrease in protein levels occurred in a dose dependent manner compared to untreated cells, suggesting that *IRAK1* protein levels reduced in response to miR-146a-NPs.

To determine miR-146a-NPs biological function, the IL-8 promoter reporter assay was used. The pIL-8 promoter- GFP reporter was transfected into A549 cells, which express the functional IL-1 receptors [24]. The promoter's response after IL-1β stimulation produced intense fluorescent signal (Fig. 7Ci), while IL-8 promoter reporter output (GFP) was dampened by miR-146a-NPs (Fig. 7Cii).

4. Discussion

4.1. Optimization of cationic NPs

The data presented in this study indicate that PGA-co-PDL mixed with DOTAP formed cationic NPs using 10–25% (w/w) DOTAP. It was noted that increasing the concentration of DOTAP decreased particle size and caused the zeta potential to become more positive (Fig. 1A). This data agrees with previous research indicating that the use of DOTAP during particle preparation affects the particle size. Jensen *et al.* used DOTAP with PLGA for siRNA delivery, and reported that particle size decreased from 260.8 ± 14.1 nm to 207.7 ± 0.1 nm after use of various DOTAP concentrations, included during preparation [15].

DOTAP has previously been used in other studies as a cationic material to modify polymeric NP properties such as particle size, charge and improve gene transfection [25]. DOTAP is thought to limit the enlargement of polymeric NPs due to its surfactant and condensation characteristics [15]. Another reason for the change in particle size is that the cationic material has the ability to decrease interfacial tension between the particle surface and the aqueous phase during formation [26]. This is similar to the effect of PVA on particle size during preparation of NPs [27], where the particle size decreased due to an adequate amount of surfactant covering the surface of PGA-co-PDL NPs [20]. Furthermore, electrostatic interaction between the DOTAP cationic moiety, quaternary amine and the negatively charged PGA-co-PDL neutralises the PGA-co-PDL and the remaining amine groups cause the positive charge [28–30].

The particle surface charge is another important factor for miRNA adsorption and cellular uptake. This electrostatic surface charge affects the adsorption of miR-146a, and addition of negatively charged miR-146a lead to a slight charge reduction in cationic NPs. This could be attributed to the decreased surface area of cationic NPs and ionic interactions [23,31]. The charge of cationic NPs remained positive after miR-146a adsorption, and the amount of miR-146a adsorbed on cationic NPs over different time points indicated that the surface of cationic NPs was saturated with miR-146a after 2 h (Fig. 1B–D).

4.2. In vitro release

The *in vitro* release of miR-146a from 15% DOTAP NPs is affected by the presence of DOTAP in NPs. Cationic DOTAP has a quaternary amine group that provides opportunity of intermolecular hydrogen bonding with PVA and PGA-co-PDL, so DOTAP forms a network on the particle's surface which affects miR-146a release. A similar study with surface adsorbed siRNA revealed, the *in vitro* release of siRNA from cationic PLGA was more than 60% over 24 h [32] whereas in our study more than 70% miR-146a was released from cationic NPs after 24 h. This could be related to PGA-co-PDL degrading slower than PLGA [33]. Kunda et al. conducted a similar *in vitro* release study using PGA-co-PDL NPs adsorbed BSA protein, and found that more than 90% of BSA was released because of weaker hydrophobic interactions between BSA and NPs [20].

The *in vitro* release of miR-146a after 24 h was 77 ± 1.5%, which correlated with the change in gene silencing and protein levels indicated in the Western Blot data (Fig. 7B), suggesting that miR-146a maintained its biological efficacy and was not affected by the degradation of NPs. The protein level bands were intense at lower miR-146a-NPs concentration and the bands of intensity decreased when NPs concentration is increased. The difference in protein level bands indicate that miR-146a-NPs produce intense bands which indicates a slight decrease in protein level, whereas the less intense band caused a significant decrease in protein levels, which will be discussed further in Western Blot data. A similar study by Li *et al.* using DOTAP as a cationic lipid to modify single-walled carbon nanotube as non-viral siRNA delivery system, found that cationic DOTAP electrostatically interact with negatively charged siRNA, protecting siRNA against degradation, and

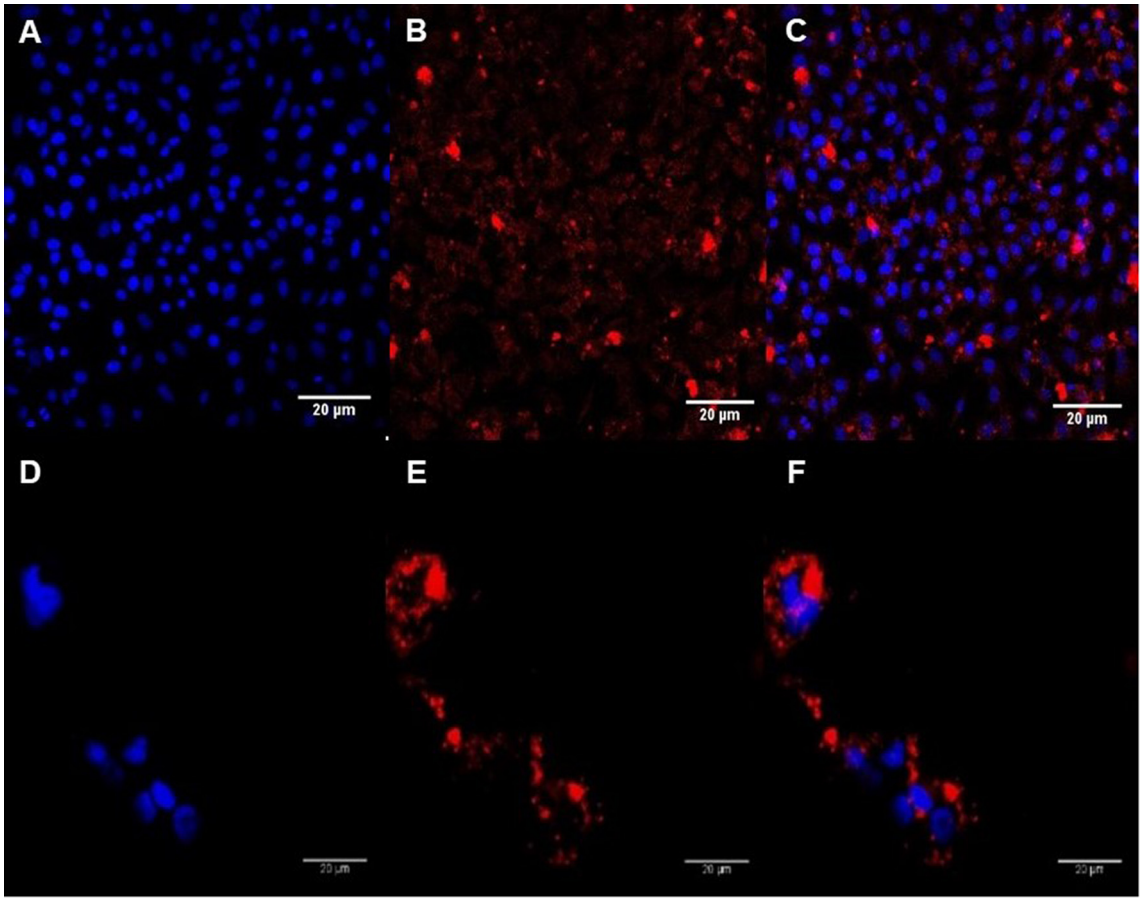

Fig. 5. Fluorescence (A–C) and confocal (D–F) images of Nile Red NPs in A549 cells after 1 h of incubation. (A&D) Nucleus is stained with DAPI, (B&E) NPs stained with Nile Red dye and (C&F) merged image. The scale bar represent 20 µm.

was released from single-walled carbon nanotube-DOTAP, realising its gene silencing potential in the cancer cells [34,35].

4.3. Cytotoxicity studies and cellular uptake

The concentration of optimum 15% DOTAP NPs caused changes in A549 cell viability ranging from 77 to 64% at 0.156–1.25 mg/ml (Fig. 4). Cells exposed to NPs without DOTAP had 96% viability at 0.312 mg/ml, which decreased to 77% with 15% DOTAP NPs at 0.312 mg/ml and 64% at 1.25 mg/ml. Although the data suggests a decrease in viability ranging from 77 to 64 %, the data obtained is with high particle concentration in a relatively small surface area (i.e. in a 96 well plate), whereas in the lungs, the surface area is significantly larger and the NPs will be more dispersed, thus the high level of NPs toxicity shown here is unlikely to be seen in a physiological setting [13]. Bose *et al.* also found that different DOTAP concentrations, when added to lipid polymer hybrid nanospheres, affected cell viability of various cell types (HEK293, HeLa, HaCaT, and HepG2) but did not cause severe cytotoxicity (cell viability was > 70% for all cell types) [23]. In addition, similar to our findings, Jensen *et al.* demonstrated the cell viability of H1229 cells was PLGA NPs and DOTAP concentration dependent with cell viability in the range of 65–70 % for 15% DOTAP-containing NPs [15].

Nile Red NP were used to show the ability of cationic NPs cellular uptake and to deliver miR-146a to the cell. The uptake of PGA-co-PDL polymer based NPs had previously demonstrated in A549 [13] and dendritic cells [17]. Conventionally, miRNA are very limited in their ability to cross the cellular membrane, without use of polymer based carrier drug delivery system [36]. The cationic NPs, with adsorbed miR-146a, were distributed in cytoplasm and at periphery of the nucleus region in A549 lung fibroblasts. This distribution of FAM labelled miR-146a suggest that miR-146a could interact with RISC complex with AGO2 and target mRNA in cytoplasm and achieve a good level of gene silencing [37,38].

4.4. Functional evaluation of miR-146a-loaded NPs on target gene, protein expression and reporter assay

The functional activity of miR-146a loaded NPs, was assessed on miR-146a target gene, *IRAK1*. Early work by Baltimore and colleagues indicated that miR-146a inhibits the expression of *IRAK1* genes and the significant function of miR-146a as negative regulator of inflammation [11]. The reduced target gene *IRAK1* of miR-146a-NPs suggest that NPs delivered miR-146a to site of action and produced the expected downregulation effect (Fig. 7A). Assessment of the impact of the miR-146a-NPs on *IRAK1* protein levels revealed protein band intensity decreased when the NPs' concentration was further increased, suggesting that NPs delivered miR-146a to site of action (Fig. 7B). These functional studies confirm that miR-146a-NPs delivered to site of action in the lung cell lines, and miR-146a have modulated both genes and protein levels [39]. With these results, miR-146a-NPs appeared to be a promising therapeutic approach for treatment of disease by targeting genes products associated with inflammation.

The effect of miR-146a-NPs in the expression of target gene *IRAK1*, protein levels, pIL-8 promoter reporter assay was used (Fig. 7C). Several studies have shown that miR-146a targets IRAK1 and TRAF6 in the IL-1R/TLR pathways that activate the NF-κB [10,11,40]. Using a fluorescent NF-κB responsive reporter, we showed that miR-146a-NPs impaired cytokine-dependent activation of NF-κB IN A549 cells. Hence, the ability of miR-146a-NPs to suppress IRAK1 translated into reduced

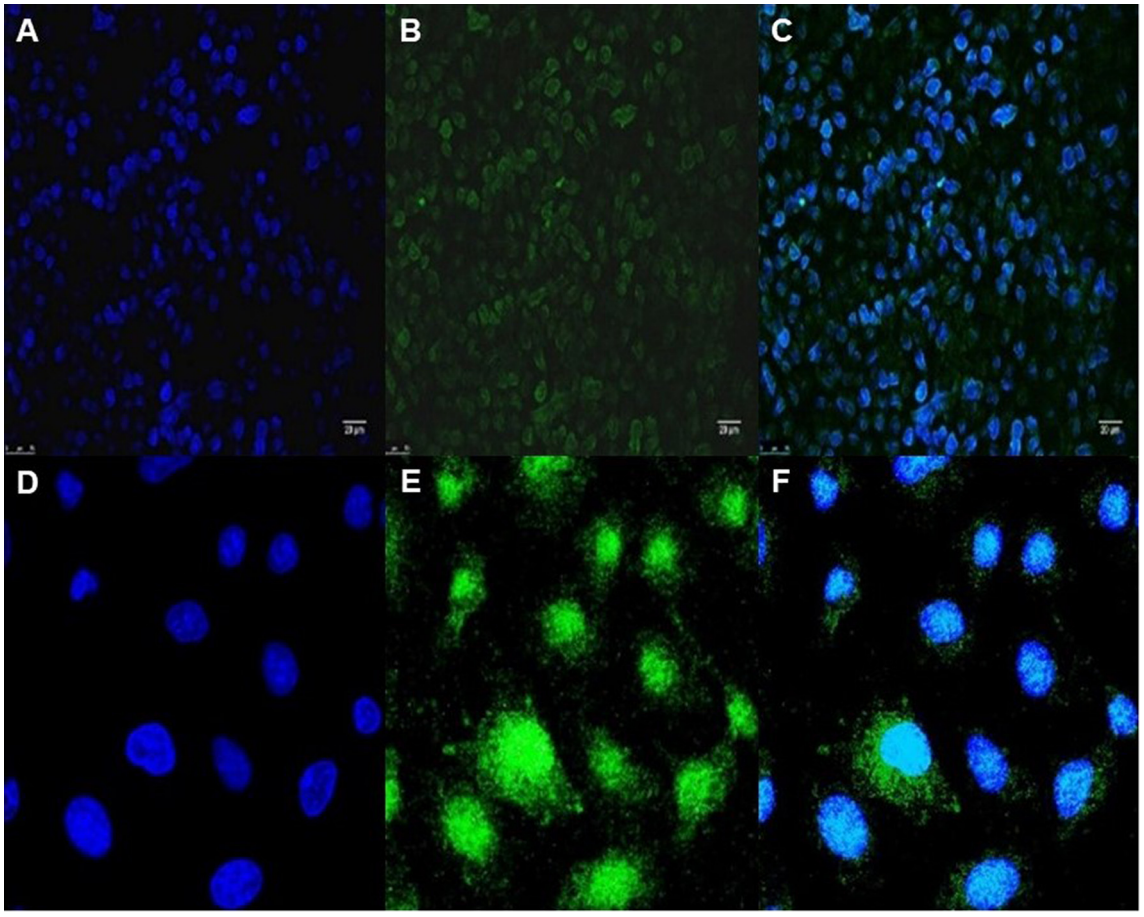

Fig. 6. Fluorescence (A–C) and confocal (D–F) images of FAM-labelled miR-146a-NPs in A549 Cells after 1 h of incubation. (A&D) Nucleus is stained with DAPI, (B& E) FAM-labelled miR-146a-NPs and (C&F) merged image. The scale bar represent 20 μm.

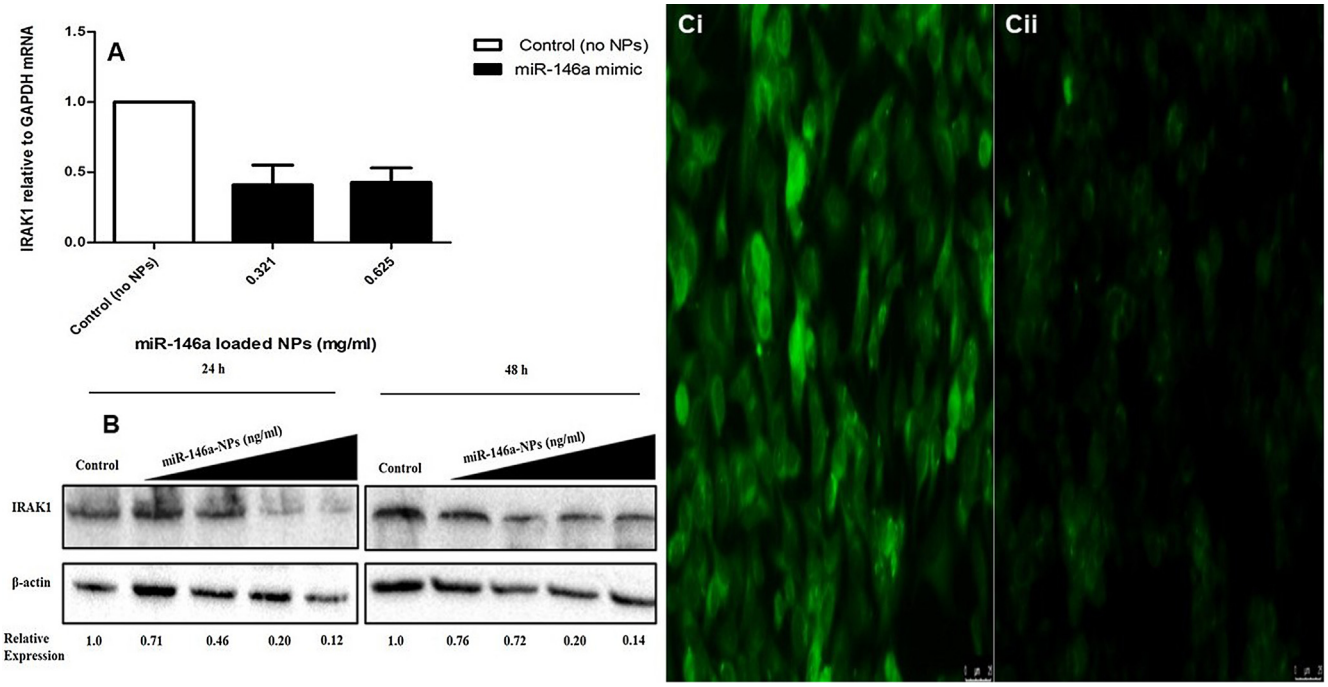

Fig. 7. (A) Effect of miR-146a loaded NPs on IRAK1 expression. The highest two concentrations were pooled from the three independent experiments. The expression of IRAK1 was normalised to GAPDH expression. Data represented as Mean ± SD (n = 3). (B) Effect of miR-146a on IRAK1 protein levels in A549 cells. Dark triangle represents lowest (left) to highest (right) miR-146a-NPs concentrations. The numbers under each band represents the densitometric readings relative to control samples normalized to each band and to its corresponding β-actin control. Fluorescence images of (Ci) response of pIL8 reporter to cells stimulated with IL-1β, (Cii) Cells loaded with miR-146a-NPs prior to stimulation with IL-1β. The scale bar represent 20 μm.

activation of NF-κB and may thus ameliorate inflammatory processes associated with COPD. However, evaluation of the miR-146a-NPs in patient-derived COPD alveolar cells in monolayer and three-dimensional cultures will be required to demonstrate the full clinical potential of miR-146a-NPs. In human alveolar epithelial lung cells miR-146a reduced expression of IRAK1 [9].

5. Conclusion

The cationic DOTAP was successfully used to produce cationic NPs with particle size 244.8 ± 4.4 nm, which was similar to unloaded NPs 242.4 ± 0.3 nm. Moreover, cationic NPs offer positive surface charge for miR-146a adsorption. The miR-146a adsorption was 32.25 ± 2.0 μg miR-146a per 10 mg NPs after 2 h (the optimum conditions were 15% DOTAP and miR146a adsorbed after 2 h). The *in vitro* release of miR-146a after 24 h was 77 ± 1.5%, the NPs were taken up by the cells and delivered miR-146a into the cell.

The miR-146a maintained its functional structure under gene silencing and protein level. The high miR-146a-NPs concentration reduced target gene *IRAK1* expression to 40%. The miR-146a-NPs reduced IL-8 promoter reporter GFP via IL-1β signalling pathway suggestion that miR-146a-NPs can be used to target proteins, regulate the inflammatory process. These successful studies and results show the potential of cationic NPs for delivery of miR-146a in the treatment and management of COPD.

References

[1] J. Vestbo, S.S. Hurd, A.G. Agustí, P.W. Jones, C. Vogelmeier, A. Anzueto, P.J. Barnes, L.M. Fabbri, F.J. Martinez, M. Nishimura, Global strategy for the diagnosis, management, and prevention of chronic obstructive pulmonary disease: GOLD executive summary, Am. J. Respir. Crit. Care Med. 187 (2013) 347–365.

[2] C.F. Vogelmeier, G.J. Criner, F.J. Martinez, A. Anzueto, P.J. Barnes, J. Bourbeau, B.R. Celli, R. Chen, M. Decramer, L.M. Fabbri, Global strategy for the diagnosis, management, and prevention of chronic obstructive lung disease 2017 report. GOLD executive summary, Am. J. Respir. Crit. Care Med. 195 (2017) (2017) 557–582.

[3] R.A. Pauwels, A.S. Buist, P.M. Calverley, C.R. Jenkins, S.S. Hurd, Global strategy for the diagnosis, management, and prevention of chronic obstructive pulmonary disease, Am. J. Respir. Crit. Care Med. 163 (2012) 1256–1276.

[4] S.W. Eichhorn, H. Guo, S.E. McGeary, R.A. Rodriguez-Mias, C. Shin, D. Baek, S.-H. Hsu, K. Ghoshal, J. Villén, D.P. Bartel, mRNA destabilization is the dominant effect of mammalian microRNAs by the time substantial repression ensues, Mol. Cell 56 (2014) 104–115.

[5] Y. Fujita, F. Takeshita, K. Kuwano, T. Ochiya, RNAi therapeutic platforms for lung diseases, Pharmaceuticals 6 (2013) 223–250.

[6] A. Kishore, J. Borucka, J. Petrkova, M. Petrek, Novel insights into miRNA in lung and heart inflammatory diseases, Mediators Inflamm. 2014 (2014) 259131.

[7] A. Ebrahimi, E. Sadroddiny, MicroRNAs in lung diseases: recent findings and their pathophysiological implications, Pulm. Pharmacol. Ther. 34 (2015) 55–63.

[8] T. Sato, X. Liu, A. Nelson, M. Nakanishi, N. Kanaji, X. Wang, M. Kim, Y. Li, J. Sun, J. Michalski, Reduced miR-146a increases prostaglandin E2 in chronic obstructive pulmonary disease fibroblasts, Am. J. Respir. Crit. Care Med. 182 (2010) 1020–1029.

[9] M.M. Perry, S.A. Moschos, A.E. Williams, N.J. Shepherd, H.M. Larner-Svensson, M.A. Lindsay, Rapid changes in microRNA-146a expression negatively regulate the IL-1β-induced inflammatory response in human lung alveolar epithelial cells, J. Immunol. 180 (2008) 5689–5698.

[10] D. Bhaumik, G.K. Scott, S. Schokrpur, C.K. Patil, A.V. Orjalo, F. Rodier, G.J. Lithgow, J. Campisi, MicroRNAs miR-146a/b negatively modulate the senescence-associated inflammatory mediators IL-6 and IL-8, Aging 1 (2009) 402–411.

[11] K.D. Taganov, M.P. Boldin, K.-J. Chang, D. Baltimore, NF-κB-dependent induction of microRNA miR-146, an inhibitor targeted to signaling proteins of innate immune responses, Proc. Natl. Acad. Sci. USA 103 (2006) 12481–12486.

[12] D. Guzman-Villanueva, I.M. El-Sherbiny, D. Herrera-Ruiz, A.V. Vlassov, H.D. Smyth, Formulation approaches to short interfering RNA and MicroRNA: challenges and implications, J. Pharm. Sci. 101 (2012) 4046–4066.

[13] N.K. Kunda, I.M. Alfagih, S.R. Dennison, S. Somavarapu, Z. Merchant, G.A. Hutcheon, I.Y. Saleem, Dry powder pulmonary delivery of cationic PGA-co-PDL nanoparticles with surface adsorbed model protein, Int. J. Pharm. 492 (2015) 213–222.

[14] J.J. Green, E. Chiu, E.S. Leshchiner, J. Shi, R. Langer, D.G. Anderson, Electrostatic ligand coatings of nanoparticles enable ligand-specific gene delivery to human primary cells, Nano Lett. 7 (2007) 874–879.

[15] D.K. Jensen, L.B. Jensen, S. Koocheki, L. Bengtson, D. Cun, H.M. Nielsen, C. Foged, Design of an inhalable dry powder formulation of DOTAP-modified PLGA nanoparticles loaded with siRNA, J. Control. Release 157 (2012) 141–148.

[16] H. Li, Y. Hao, N. Wang, L. Wang, S. Jia, Y. Wang, L. Yang, Y. Zhang, Z. Zhang, DOTAP functionalizing single-walled carbon nanotubes as non-viral vectors for efficient intracellular siRNA delivery, Drug Deliv. 23 (2016) 840–848.

[17] I. Alfagih, N. Kunda, F. Alanazi, S.R. Dennison, S. Somavarapu, G.A. Hutcheon, I.Y. Saleem, Pulmonary delivery of proteins using nanocomposite microcarriers, J. Pharm. Sci. 104 (2015) 4386–4398.

[18] T.C. Rodrigues, M.L.S. Oliveira, A. Soares-Schanoski, S.L. Chavez-Rico, D.B. Figueiredo, V.M. Goncalves, D.M. Ferreira, N.K. Kunda, I.Y. Saleem, E.N. Miyaji, Mucosal immunization with PspA (Pneumococcal surface protein A)-adsorbed nanoparticles targeting the lungs for protection against pneumococcal infection, PloS one 13 (2018) e0191692.

[19] N.K. Kunda, I.M. Alfagih, E.N. Miyaji, D.B. Figueiredo, V.M. Goncalves, D.M. Ferreira, S.R. Dennison, S. Somavarapu, G.A. Hutcheon, I.Y. Saleem, Pulmonary dry powder vaccine of pneumococcal antigen loaded nanoparticles, Int. J. Pharm. 495 (2015) 903–912.

[20] N.K. Kunda, I.M. Alfagih, S.R. Dennison, H.M. Tawfeek, S. Somavarapu, G.A. Hutcheon, I.Y. Saleem, Bovine serum albumin adsorbed PGA-co-PDL nanocarriers for vaccine delivery via dry powder inhalation, Pharm. Res. 32 (2015) 1341–1353.

[21] K.J. Livak, T.D. Schmittgen, Analysis of relative gene expression data using real-time quantitative PCR and the $2-\Delta\Delta CT$ method, Methods 25 (2001) 402–408.

[22] D. Fischer, Y. Li, B. Ahlemeyer, J. Krieglstein, T. Kissel, In vitro cytotoxicity testing of polycations: influence of polymer structure on cell viability and hemolysis, Biomaterials 24 (2003) 1121–1131.

[23] R.J. Bose, Y. Arai, J.C. Ahn, H. Park, S.-H. Lee, Influence of cationic lipid concentration on properties of lipid–polymer hybrid nanospheres for gene delivery, Int. J. Nanomed. 10 (2015) 5367–5382.

[24] G.J. Ding, P.A. Fischer, R.C. Boltz, J.A. Schmidt, J.J. Colaianne, A. Gough, R.A. Rubin, D.K. Miller, Characterization and quantitation of NF-κB nuclear translocation induced by interleukin-1 and tumor necrosis factor-α development and use of a high capacity fluorescence cytometric system, J. Biol. Chem. 273 (1998) 28897–28905.

[25] M.R. Kumar, U. Bakowsky, C. Lehr, Preparation and characterization of cationic PLGA nanospheres as DNA carriers, Biomaterials 25 (2004) 1771–1777.

[26] K.C. Song, H.S. Lee, I.Y. Choung, K.I. Cho, Y. Ahn, E.J. Choi, The effect of type of organic phase solvents on the particle size of poly (D, L-lactide-co-glycolide) nanoparticles, Colloids Surf. A Physicochem. Eng. Asp. 276 (2006) 162–167.

[27] H. Murakami, Y. Kawashima, T. Niwa, T. Hino, H. Takeuchi, M. Kobayashi, Influence of the degrees of hydrolyzation and polymerization of poly (vinylalcohol) on the preparation and properties of poly (DL-lactide-co-glycolide) nanoparticle, Int. J. Pharm. 149 (1997) 43–49.

[28] T. Hagigit, T. Nassar, F. Behar-Cohen, G. Lambert, S. Benita, The influence of cationic lipid type on in-vitro release kinetic profiles of antisense oligonucleotide from cationic nanoemulsions, Eur. J. Pharm. Biopharm. 70 (2008) 248–259.

[29] R.B. Campbell, S.V. Balasubramanian, R.M. Straubinger, Phospholipid-cationic lipid interactions: influences on membrane and vesicle properties, Biochim. Biophys. Acta 1512 (2001) 27–39.

[30] S. Mura, H. Hillaireau, J. Nicolas, B. Le Droumaguet, C. Gueutin, S. Zanna, N. Tsapis, E. Fattal, Influence of surface charge on the potential toxicity of PLGA nanoparticles towards Calu-3 cells, Int. J. Nanomed. 6 (2011) 2591–2605.

[31] A. Kumar, P. Wonganan, M.A. Sandoval, X. Li, S. Zhu, Z. Cui, Microneedle-mediated transcutaneous immunization with plasmid DNA coated on cationic PLGA nanoparticles, J. Control. Release 163 (2012) 230–239.

[32] H.V. Jagani, V.R. Josyula, V.R. Palanimuthu, R.C. Hariharapura, S.S. Gang, Improvement of therapeutic efficacy of PLGA nanoformulation of siRNA targeting anti-apoptotic Bcl-2 through chitosan coating, Eur. J. Pharm. Sci. 48 (2013) 611–618.

[33] H. Tawfeek, S. Khidr, E. Samy, S. Ahmed, M. Murphy, A. Mohammed, A. Shabir, G. Hutcheon, I. Saleem, Poly (glycerol adipate-co-ω-pentadecalactone) spray-dried microparticles as sustained release carriers for pulmonary delivery, Pharm. Res. 28 (2011) 2086–2097.

[34] H. Li, Y. Hao, N. Wang, L. Wang, S. Jia, Y. Wang, L. Yang, Y. Zhang, Z. Zhang, DOTAP functionalizing single-walled carbon nanotubes as non-viral vectors for efficient intracellular siRNA delivery, Drug Deliv. 23 (2016) 830–838.

[35] D.J. Gibbings, C. Ciaudo, M. Erhardt, O. Voinnet, Multivesicular bodies associate with components of miRNA effector complexes and modulate miRNA activity, Nat. Cell Biol. 11 (2009) 1143–1149.

[36] H. Yin, R.L. Kanasty, A.A. Eltoukhy, A.J. Vegas, J.R. Dorkin, D.G. Anderson, Non-viral vectors for gene-based therapy, Nat. Rev. Genet. 15 (2014) 541–555.

[37] Y. Wu, M. Crawford, Y. Mao, R.J. Lee, I.C. Davis, T.S. Elton, L.J. Lee, S.P. Nana-Sinkam, Therapeutic delivery of microRNA-29b by cationic lipoplexes for lung cancer, Mol. Ther. Nucleic Acids. 2 (2013) e84.

[38] C.D. Kuhn, L. Joshua-Tor, Eukaryotic Argonautes come into focus, Trends Biochem. Sci. 38 (2013) 263–271.

[39] M.E. Ezzie, M. Crawford, J.H. Cho, R. Orellana, S. Zhang, R. Gelinas, K. Batte, L. Yu, G. Nuovo, D. Galas, P. Diaz, K. Wang, S.P. Nana-Sinkam, Gene expression networks in COPD: microRNA and mRNA regulation, Thorax 67 (2012) 122–131.

[40] R. Saba, D.L. Sorensen, S.A. Booth, MicroRNA-146a: a dominant, negative regulator of the innate immune response, Front. Immunol. 5 (2014) 578.